

Sustainable magnetically recoverable Iridium coated Fe_3O_4 nanoparticles for enhanced catalytic reduction of organic pollutants in water

Diksha kumari

Punjab Engineering College

Manpreet Kaur

Punjab Engineering College

Veeranna Yempally

Punjab Engineering College

Harminder Kaur (✉ hkaur@pec.edu.in)


Punjab Engineering College

Research Article

Keywords: Photocatalyst, synergism, reduction of nitroaromatics, sustainable magnetic nanocatalyst, Ir nanoparticles, recyclability

Posted Date: June 13th, 2022

DOI: <https://doi.org/10.21203/rs.3.rs-1750046/v1>

License:  This work is licensed under a Creative Commons Attribution 4.0 International License. [Read Full License](#)

Abstract

In the present study, modified Fe_3O_4 nanoparticles were fabricated by surface coating with tryptophan and Iridium by co-precipitation method to afford $\text{Fe}_3\text{O}_4@\text{trp}@\text{Ir}$ magnetic nanoparticles. As-prepared $\text{Fe}_3\text{O}_4@\text{trp}@\text{Ir}$ nanoparticles are environmentally benign efficient catalysts for reducing organic pollutants such as 4-nitrophenol (4-NP), 4-nitroaniline (4-NA), and 1-bromo-4-nitrobenzene (1-B-4-NB). The key parameters that affect the catalytic activity like temperature, catalyst loading, and the concentration of reducing agent NaBH_4 were optimized. The obtained results proved that $\text{Fe}_3\text{O}_4@\text{trp}@\text{Ir}$ is an efficient catalyst for reducing nitroaromatics at ambient temperature with a minimal catalyst loading of 0.0025%. The complete conversion of 4-nitrophenol to 4-aminophenol took only 20 seconds with a minimal catalyst loading of 0.0025% and a rate constant of 0.0522 s^{-1} . The high catalytic activity factor ($1.040 \text{ s}^{-1}\text{mg}^{-1}$) and high turnover frequency (9 min^{-1}) obtained for $\text{Fe}_3\text{O}_4@\text{trp}@\text{Ir}$ nanocatalyst highlight the possible synergistic effect of the two metals (Fe and Ir). The visible-light photocatalytic degradation of 4-NP was also investigated in the presence of $\text{Fe}_3\text{O}_4@\text{trp}@\text{Ir}$. The photocatalytic degradation of 4-NP by $\text{Fe}_3\text{O}_4@\text{trp}@\text{Ir}$ is completed in 20 min with 95.15% efficiency, and the rate of photodegradation of 4-NP (0.1507 min^{-1}) is about twice the degradation rate of 4-NP in the dark (0.0755 min^{-1}). The catalyst was recycled and reused for five cycles without significant reduction in the conversion efficiency of the catalyst.

Introduction

The nanosized noble metal oxides have been garnering widespread attention in recent years owing to their unique chemical and physical properties over their bulk counterparts and their applications in fields of catalysis, optics, electronics, etc (Chi et al. 2012; Fagiolari et al. 2020). Iridium nanocatalysts (Ir NPs) have demonstrated excellent catalytic activity in water splitting, hydrogen evolution reaction (HER), and oxygen reduction reaction (ORR), and other redox-reactions (Feng et al. 2017; Ohno et al. 2017; Zhang et al. 2020). However, their applications in the reduction of nitroaromatics has received little attention (Xu et al. 2015; Cui et al. 2020; Thekkathu et al. 2020). Despite the excellent catalytic activity and corrosion resistivity of Ir-based nanocatalysts, their use in the hydrogenation of nitroarenes has not been explored rigorously. Specifically, the photocatalytic reduction of nitroaromatics using the iridium nanoparticles or homogeneous Ir catalysts has been scarcely reported. Moreover, large-scale industrial use of Ir NPs is limited due to their high cost, difficulty in separation, limited supply, and their tendency to undergo aggregation. Reducing the amounts of the catalyst used and improving the catalytic efficiency are among the top priorities for their large-scale practical applications in industries. There is a huge scope to design and develop efficient and highly active Ir nano-catalysts for application in the reduction of nitroaromatics under mild reaction conditions (Cui et al. 2020).

The conventional way to increase the catalytic activity is by deposition of Ir NPs on porous solid supports such as TiO_2 , SiO_2 , carbon, etc (Kapkowski et al. 2017; Muntean et al. 2019). However, immobilizing nanocatalysts on solid supports suffers from the limitation of decreasing the active surface area of the catalyst and difficulty in recycling thus hindering the catalyst recovery and reusability in aqueous solutions. The use of magnetite nanoparticles as environment-friendly and easily available support can help in overcoming the above limitations (Tie et al. 2006; Theerdhala et al. 2010; Nasir Baig and Varma 2013; Banerjee et al. 2018). Magnetic Fe_3O_4 nanoparticles as support provide stability, reduce the overall cost, enhance recyclability and make the separation process easy (Nasir Baig and Varma 2013).

The nitroaromatics such as 4-NP, 4-NA, and 1-B-4-NB are organic pollutants found in industrial effluents which contaminate the groundwater and cause harm to both humans and aquatic life (Hung et al. 2016; Basavegowda et al. 2017; Mondal et al. 2017; Cui et al. 2020). Aromatic amines obtained from the reduction of nitroaromatics are not only less toxic than nitroaromatics but also act as important intermediates in the synthesis of dyes, drugs, pigments, herbicides, and polymers (Veisi et al. 2019; Rawat et al. 2021). Recently, Thekkathu and co-workers reported a

magnetically recoverable Iridium nanocatalyst supported on a silica shell for nitrophenols reduction (Thekkathu et al. 2020). Although these materials possess improved stability and enhanced recyclability, the procedures for synthesis are complicated and involve multiple steps. The surface coating with silica shell not only enhances the diameter of the synthesized nanoparticles but also causes a reduction in the magnetic property. A feasible option involves the direct functionalization of magnetic nanoparticles with biocompatible molecules such as amino acids (AA) (Tie et al. 2006). AA not only possesses active groups for interaction with different biological molecules but also provides colloidal stability to the MNPs (Pav et al. 2020). The carboxylic acid functional group of AA can be efficiently grafted on Fe_3O_4 and nitrogen donor atoms of AA can participate in the coordination to the noble metal centers (Ir, Pt, Ag etc) to produce stable metal complexes for application in catalysis. For example, Jain et al. recently reported immobilization of Ag NPs on the Fe_3O_4 @glutathione super magnetic nanoparticles (Kumari et al. 2019) for the reduction of nitroarenes. The Fe_3O_4 -Glu-Ag NPs were efficient in reduction of 4-NP even in the gram scale employing water as solvent, and NaBH_4 as reducing agent providing the pathway for development of green catalysts for application in the industry (Kumari et al. 2019).

Photocatalysis under visible light irradiation is one of the rapidly developing techniques that can be employed for the degradation of organic pollutants, dyes, and drugs (Mohamed and Al-Sharif 2013; Kianfar and Arayesh 2020). Fe_3O_4 nanocomposites possess a narrow bandgap, superior magnetism, and their ability to effectively transport photogenerated electrons making them ideal candidates for visible light photocatalysis (Dinari and Dadkhah 2021). Over the past decade, the Fe_3O_4 nanocomposites decorated with different noble metals are employed in photodegradation of nitroaromatics (Seoudi and Al-Marhaby 2016; Samuel et al. 2020). The photocatalytic efficiency of the synthesized nanocatalyst can also be improved by incorporating noble metals in the nanocomposite. The incorporation of noble metals enhances the light absorption ability of the photocatalyst due to the surface plasmon resonance (SPR) effect of noble metals (Pham et al. 2021). We have decided to exploit this strategy further by immobilization of Iridium metal on the surface of tryptophan (AA) grafted Fe_3O_4 nanoparticles. We anticipate that tryptophan AA anchored on the surface of Fe_3O_4 will enhance the stability of magnetic nanoparticles towards surface oxidation, and efficiently reduce the agglomeration of iridium nanoparticles (Dhanalakshmi et al. 2020; Alaghmandfard and Madaah Hosseini 2021; Belachew et al. 2021). The Iridium NPs as photocatalysts for various redox reactions is well known (Babajani and Jamshidi 2019; Dhanalakshmi et al. 2020). The application of Iridium NPs as catalysts in nitroarenes reduction is also gaining momentum recently (Xu et al. 2015; Goel and Lasyal 2016; Yan et al. 2017). We hypothesize that the presence of iridium on the surface of Fe_3O_4 @trp@Ir will definitely aid in photocatalytic reduction of organic pollutants, specifically nitroaromatics. The primary aim of the present work is to develop a robust environmentally benign catalyst (Fe_3O_4 @trp@Ir) for the rapid reduction of nitroarenes under mild reaction conditions. A simple and effective approach for the fabrication of Fe_3O_4 @trp@Ir nanoparticles is reported in this work. The generated nanocatalyst's catalytic efficiency was demonstrated in the elimination of different organic pollutants by NaBH_4 in an aqueous medium.

Experimental Section

Materials

Ferric chloride ($\text{FeCl}_3 \cdot 6\text{H}_2\text{O}$) was purchased from Alfa Aesar and Ferrous sulphate ($\text{FeSO}_4 \cdot 7\text{H}_2\text{O}$) was obtained from Fischer Scientific. $\text{IrCl}_3 \cdot 3\text{H}_2\text{O}$ (Sigma Aldrich), 4-nitrophenol (Sigma Aldrich), 4-nitroaniline (Sigma Aldrich), 1-Bromo-4-nitrobenzene (Sigma Aldrich), NaBH_4 (Alfa Aesar) were used as received without further purification. The synthesis process was carried out in de-ionized (DI) water.

Instrumentation

The UV-Visible absorption spectra were recorded using Systronics Double beam Spectrophotometer 2203. The as-prepared Fe₃O₄@trp, Fe₃O₄@trp@Ir nanocatalysts were characterized by Fourier transform infrared spectroscopy (FTIR, Perkin Elmer Spectrum Two spectrometer) and X-ray diffraction (XRD, Bruker Model D8-Advance, Cu anode, 40 kV, 40 mA). The particle size and surface morphologies were obtained using transmission electron microscopy (TEM, JEOL JEM-F200); field emission scanning electron microscopy (FESEM, Model JSM6100 Jeol). The elemental composition was determined by X-ray photoelectron spectroscopy (XPS, Physical Electronics, and Model PHI 5000 VersaProbe III). The specific surface areas of Fe₃O₄@trp@Ir nanocatalyst were determined by Brunauer-Emmett-Teller (BET, Quantachrome). A vibrating sample magnetometer (VSM, Lake Shore Model- 7410 Series) was used to determine the magnetic of synthesized nanocatalysts. The zeta potential of nanoparticles was measured by Zeta potential analyzer (Malvern Zetasizer Nano ZS).

Preparation of Fe₃O₄@trp

Direct co-precipitation method was adopted for the preparation of Fe₃O₄@trp with slight modification (Moeini et al. 2018). It was synthesized by mixing Fe²⁺ (2 mmol) and Fe³⁺ (4 mmol) salts in 50 mL distilled water and agitated continuously for 30 min under nitrogen atmosphere before the addition of 8 mmol tryptophan. Stirring was continued for another 30 min followed by the addition of 5 mL of NH₃ solution. The reaction mixture was stirred for another 1.5 h, Fe₃O₄@trp precipitates were collected using a super magnet, washed with methanol (20 mL × 1), and deionized water (20 mL × 3), and dried in an oven at 80 °C for 24 h.

Preparation of Fe₃O₄@trp@Ir

Fe₃O₄@trp (300 mg) was dispersed in distilled water (80 mL) by ultrasonication. Solution of IrCl₃.3H₂O (10 mg) in water (20 mL) was added to the above solution and stirring was continued for 12 h. Freshly prepared NaBH₄ solution was added to reduce Ir(III) ions to Ir(0). Stirring was further continued for 3 h and precipitates were separated magnetically, washed with deionized water (20 mL×3) and ethanol (20 mL×3), and dried in an oven at 80°C to obtain Fe₃O₄@trp@Ir nanoparticles.

Catalytic Reduction of 4-NP, 4-NA, and 1-B-4-NB using Fe₃O₄@trp@Ir nanocatalyst

The catalytic activity of the formed nanocatalyst for the reduction of nitroarenes was investigated using 4-Nitrophenol as a model substrate (Dutta et al. 2014). Stock solution of 10⁻² M 4-Nitrophenol was prepared and kept in dark. 0.1 M NaBH₄ solution was freshly prepared before the experiment. 30 µl of 4-NP (10⁻² M) and 0.3 mL of NaBH₄ solution (0.1 M) were diluted to 3 mL followed by the addition of 0.1 mg/mL of the nanocatalyst where the final concentration of 4-NP, NaBH₄, and the final nanocatalyst became 7.4×10⁻⁵ M, 0.0074 M and 0.025 mg/mL respectively. The progress of the reaction was monitored with time by recording UV-Visible spectra. After the reaction, the catalyst was recovered using an external magnet and washed several times with ethanol and distilled water before utilizing it for the next catalytic cycle.

Photocatalytic Reduction of 4-NP using Fe₃O₄@trp@Ir nanocatalyst

A comparative study was performed to test the photocatalytic activity of the synthesized catalyst in the reduction of 4-NP at room temperature using 200 watts LED Flood lamp ($\lambda > 400$ nm) as a source of visible light (Paul and Dhar 2020). The catalytic reduction process was carried out by the addition of 0.005 g of Fe₃O₄@trp@Ir nanocatalyst to the solution containing 50 ml of 4 NP (0.01 mmol L⁻¹) and 5 ml of NaBH₄ (0.05 M) in a beaker and stirring was continued. The kinetics of the photocatalytic reduction of 4-NP was studied by recording UV-Vis spectra of a small aliquot of the

sample at regular time intervals. The catalyst was retrieved using a magnet after the completion of the reaction and used for 5 successive cycles after washing with water and ethanol. The percentage degradation of 4-NP is given:

$$D (\%) = \left[\frac{A_0 - A}{A_0} \right] \times 100$$

Where A_0 is the absorbance of the sample before irradiation in visible light, A is the absorbance of the sample after light irradiation process (Shabib et al. 2022).

Results And Discussion

In this work, $\text{Fe}_3\text{O}_4@\text{trp}$ nanoparticles were synthesized by conventional co-precipitation method from $\text{FeSO}_4 \cdot 7\text{H}_2\text{O}$, $\text{FeCl}_3 \cdot 6\text{H}_2\text{O}$ and tryptophan in (2:4:8) ratio followed by immobilization of Iridium on the surface of $\text{Fe}_3\text{O}_4@\text{trp}$ (**Scheme 1**). The as-prepared nanoparticles were characterized by XRD, FTIR, FE-SEM, TEM, XPS, TGA, CV, VSM, PL studies, etc. The XRD pattern of Fe_3O_4 nanoparticles showed 6 characteristic diffraction peaks at $2\theta = 30.27, 35.72, 43.30, 53.99, 57.33,$ and 63.01 corresponding to the cubic inverse spinel structure of Fe_3O_4 (Moeini et al. 2018). From the XRD analysis of $\text{Fe}_3\text{O}_4@\text{trp}@Ir$ nanoparticles, no characteristic peak of Iridium in the final catalyst was obtained (**Fig.1a**). This may be due to its low loading and small peak size (Boruah et al. 2015). The average crystallite size of $\text{Fe}_3\text{O}_4@\text{trp}@Ir$ nanocatalyst estimated using the Debye-Scherrer equation was 9.3 nm.

The FTIR spectra of magnetic Fe_3O_4 nanoparticles showed strong absorption peaks at 633 and 578 cm^{-1} which were associated with Fe-O stretching vibration modes (Mihaela et al. 2022). A broad peak at 3415 cm^{-1} was assigned to stretching vibrations of adsorbed water molecules on the surface of Fe_3O_4 nanoparticles (**Fig. 1b**). Two more distinctive bands were observed in the case of $\text{Fe}_3\text{O}_4@\text{trp}$, at 1622 and 1400 cm^{-1} , which correspond to asymmetric COO^- stretching vibration and symmetric COO^- stretching vibration, respectively (Theerdhala et al. 2010). The retention of these peaks in the final catalyst proved that tryptophan remains attached even after binding with Ir nanoparticles. The surface morphology of the formed nanocatalyst and its physical properties were determined by Field emission-scanning electron microscopy (FE-SEM). The nanoparticles appeared to have spherical shape and were nearly agglomerated. (**Fig. 1c**) showed that tryptophan and Iridium were densely distributed over the whole Fe_3O_4 surface. The energy-dispersive X-ray spectrum (EDS) analysis confirmed the existence of Fe, O, C, N, and Ir in the formed nanocatalyst (**Fig. 1d**). The average diameter of $\text{Fe}_3\text{O}_4@\text{trp}@Ir$ nanocatalyst calculated from SEM micrographs was 17.3 nm whereas the average diameter of bare Fe_3O_4 nanoparticles was found to be in the range of 8-12 nm. The increase in the particle size in the final catalyst indicated successful modification of the surface of Fe_3O_4 nanoparticles (Banerjee et al. 2018).

Thermal stability and decomposition behavior of as-prepared nanoparticles were studied by thermo-gravimetric (TGA) analysis (**Fig. 1e**). The weight loss below $200 \text{ }^\circ\text{C}$ was due to adsorbed water molecules and hydroxyl groups on the surface of magnetic Fe_3O_4 nanoparticles. Decomposition of well grafted organic groups on the surface of Fe_3O_4 nanoparticles caused weight loss in the $200\text{-}600 \text{ }^\circ\text{C}$ range. After immobilization of tryptophan and Iridium on the surface of Fe_3O_4 nanoparticles, the stability of $\text{Fe}_3\text{O}_4@\text{trp}@Ir$ nanocatalyst was enhanced effectively.

At room temperature, the magnetic behavior of bare and modified Fe_3O_4 nanoparticles was studied using a Vibrating Sample Magnetometer (VSM) in the field range of $-10,000$ to $+10,000 \text{ Oe}$. (**Fig. 2a**). The magnetization saturation values (Ms) of Fe_3O_4 , $\text{Fe}_3\text{O}_4@\text{trp}$, and $\text{Fe}_3\text{O}_4@\text{trp}@Ir$ were found to be 71.11, 52.97, and 50.37 emu/g respectively. The superparamagnetic behavior of the final catalyst was clearly shown from the VSM graph with negligible remanence and coercivity. The lower Ms values obtained for $\text{Fe}_3\text{O}_4@\text{trp}$ and $\text{Fe}_3\text{O}_4@\text{trp}@Ir$ were caused by non-magnetic materials

becoming immobilized on the surface of magnetic Fe₃O₄ nanoparticles. The final catalyst showed enough saturation magnetization so that it could easily be separated using a super magnet (Sharif et al. 2019).

Cyclic voltammetry (CV) was used to record the electrochemical behavior of Fe₃O₄@trp and Fe₃O₄@trp@Ir in 0.1 M KOH solution using the ink drop coating method at a scan rate of 0.1 V/s (Tipsawat et al. 2018). Strong oxidation and reduction peaks were obtained at 1.17 V and -1.16 V respectively in Fe₃O₄@trp which were attributed to irreversible redox reactions between Fe²⁺ and Fe³⁺ (**Fig. 2b**).

Zeta Potential was used to determine the surface charge of Fe₃O₄@trp and Fe₃O₄@trp@Ir at neutral pH. The reported Zeta Potential of Fe₃O₄ nanoparticles was -35.6 mV (Hung et al. 2016). It can be seen from **Fig. 2 c** that as prepared Fe₃O₄@trp is negatively charged with a zeta potential value of -24.8 mV. The decrease in negative charge upon functionalization of Fe₃O₄ nanoparticles with tryptophan amino acid is due to the protonation of free NH₂ groups on the surface of amino acids (Pav et al. 2020). The synthesized Fe₃O₄@trp@Ir nanocatalyst is positively charged with a zeta potential of +3.02 mV (**Fig. 2 d**). As NaBH₄ is present in excess in the reduction of the 4-NP, the 4-Nitrophenolate ion formed is an anion species and is likely to be adsorbed on the positively charged nanocatalyst's surface (Aditya et al. 2017). The zeta potential value of positively charged Fe₃O₄@trp@Ir nanocatalyst also indicates rapid reaction of negatively charged molecules on the surface of the nanocatalyst.

The absorption of light by the material and movement of photon-induced holes and electrons are some of the key factors which are involved in controlling a photocatalytic reaction. These key factors are related to the electronic structure of the material (Chishti et al. 2021). The UV-VIS diffuse reflectance spectrum (DRS) of Fe₃O₄@trp and Fe₃O₄@trp@Ir is shown in **Fig. 3a**. The Uv-Visible Spectra of as prepared nanocatalyst show a strong absorption peak at 295 nm (**Fig. 3b**). The bandgap energy (E_g) of Fe₃O₄@trp and Fe₃O₄@trp@Ir as calculated from the Tauc plot was found to be 2.51 eV and 2.37 eV respectively (**Fig. 3c**). The bandgap energy is calculated using the Tauc's relation:

$$(\alpha h\nu)^n = B(h\nu - E_g)$$

where E_g is bandgap energy (eV), hν is the energy of the photon (eV), B is a constant, n is dependent on the type of electronic transition and α is the material's absorption coefficient (cm⁻¹). (Bagbi et al. 2017; Shabib et al. 2022)

The electron-hole recombination was determined using the PL Spectra **Fig. 3d**. The lower PL intensity of Fe₃O₄@trp@Ir nanocatalyst indicates a lower electron-hole recombination rate in the presence of light (Zhao et al. 2018; Mancuso et al. 2021). Thus, the synthesized nanocatalyst increased the lifetime of electron/hole pairs and causes enhanced photocatalytic activity.

The survey scan of the formed Fe₃O₄@trp@Ir nanocatalyst shows distinctive peaks of O1s (526.81 eV), and C1s (282.24 eV), Fe2p (708.82 eV), N1s (394.62 eV) and Ir4f (61.14 eV) (**Fig. 4a**). XPS spectra of Ir4f in the final nanocatalyst are marked by the presence of doublet in the region 63.2 and 62.4 eV arising from the j-j coupling or spin-orbit coupling of ground electronic states (Ir4f_{5/2} and Ir4f_{7/2}) as shown in **Fig. 4b**. The two binding energies of Ir4f in XPS spectra of Fe₃O₄@trp@Ir nanocatalyst is due to the presence of metallic Iridium (Ir⁰) (Kundu and Liang 2011). The relative atomic concentration (%) of Iridium in the synthesized Fe₃O₄@trp@Ir nanocatalyst is 0.34% as determined by XPS.

The standard Brunauer-Emmett-Teller (BET) and Barrett-Joyner-Halenda (BJH) methods were used to determine the specific surface area and porosity properties respectively (Bagbi et al. 2017). The specific surface area of Fe₃O₄ nanoparticles and Fe₃O₄@trp@Ir nanocatalyst calculated by plotting N₂ adsorption-desorption isotherm was 64.49 and 77.145 m²/g respectively (**Fig. 4c and Fig. 4d**). From **Fig. 4d**, it can be seen that the N₂ adsorption-desorption curve of as

prepared nanocatalyst is a type IV adsorption isotherm possessing mesoporous features. The presence of mesoporous structures was confirmed from the average pore diameter (10.63 nm). The total pore volume of as-synthesized nanocatalyst is 0.405 cm³/g. The presence of a large specific surface area of synthesized nanocatalyst (77.145 m²/g) significantly enhances the photocatalytic activity by providing increased no. of active sites for photodegradation (Chishti et al. 2021).

The surface morphology of the synthesized Fe₃O₄@trp@Ir nanocatalyst was also studied by TEM (**Fig. 5**). **Fig. 5a, b, and c** reveal the quasi-spherical morphology of the synthesized nanoparticles with an average diameter of 16.5 ± 1.2 nm. The particles possess narrow size distribution with sizes ranging from 8 to 25 nm and no visible change in the morphology. The surface coating of Fe₃O₄ nanoparticles with tryptophan and Iridium can be seen from the TEM images of Fe₃O₄@trp@Ir nanocatalyst. Further, EDS, FE-SEM, and XPS also support the successful coating of Fe₃O₄ nanoparticles with tryptophan and Iridium.

Catalytic Activity

The catalytic activity of formed Fe₃O₄@trp@Ir nanocatalyst was investigated by choosing 4-NP as a model substrate. The peak for 4-NP absorption at 317 nm was shifted to 400 nm upon the addition of aqueous solution of NaBH₄ (**Fig. 6(a)**). This was due to the formation of a highly stable 4-nitrophenolate anion. In time-dependent UV-Visible absorption spectra, the addition of 0.025 mg/mL of Fe₃O₄@trp@Ir nanocatalyst resulted in a decrease in peak intensity at 400 nm, and the appearance of a new peak at 295 nm attributed to 4-AP was observed. The complete reduction of 4-NP to 4-AP took 6 min and completion of the reaction was indicated with the disappearance of the peak at 400 nm (**Fig. 6b**). With the addition of 0.05 mg/mL of nanocatalyst, the conversion of 4-NP to 4-AP takes only 20 s with apparent rate constants (K_{app}) as 0.0522 s⁻¹ (**Fig. 7a**). Magnetic separation of catalyst is shown in **Fig. 6d**. In the absence of a catalyst, the absorbance of the peak at 400 nm decreased slightly, but no new absorption peak corresponding to 4-AP emerged at 295 nm. The catalytic activity of as-prepared Fe₃O₄@trp was also investigated for the reduction of 4-NP. The results obtained indicated that even after 2 hrs, only 5% conversion of 4NP to 4-AP took place. The kinetics studies indicate that the reaction catalyzed by Fe₃O₄@trp@Ir was pseudo-first order with a linear relationship obtained when ln (Co/Ct) versus time profiles were plotted (**Fig. 6c**).

The rate equation is given as: $\ln (Ct/Co) = -kt$

where Ct is the absorbance of 4-NP at time t, Co is the initial absorbance of 4-NP and k is the rate constant (Priya and Asharani 2018)

The effect of temperature on the degradation of 4-NP was studied at 40 °C, 50 °C, and 60 °C (**Table 1**). At 40 °C, the reaction was completed in 5 min with an apparent rate constant as 0.456 min⁻¹, and on increasing the temperature to 50 °C, 60 °C, the reaction was completed in 4 min with kapp as 0.4741 min⁻¹ and in 3 min with kapp as 0.7262 min⁻¹ respectively.

Table 1

Thermodynamic parameters for reducing 4-NP catalytically

Reaction Completion time (min)	Temperature (°C)	K_{app} (min ⁻¹)
5	40	0.4653
4	50	0.4741
3	60	0.7262

4-NA and 1B-4-NB are two other toxic pollutants that were degraded under the same experimental conditions as those of 4-NP. In the case of 1-Bromo-4-nitrobenzene (1B-4-NB), the reduction of 1B-4-NB to 4-bromoaniline was completed in 4 min (**Fig. 6g**). The absorption peak at 282 nm completely disappeared and a new absorption peak at 239 nm confirms the formation of 4-bromoaniline. Similarly, the reduction of 4-nitroaniline (4-NA) to 1, 4-phenylenediamine took place in 4 min (**Fig. 6e**). The absorption peak at 375 nm completely disappeared upon the addition of catalyst and the product obtained on reduction showed a peak at 305 nm which confirms the formation of 1, 4-phenylenediamine. Both reactions follow pseudo-first-order kinetics. (**Fig. 6f and 6h**). Upon increasing the synthesized nanocatalyst concentration to 0.05 mg/mL, the reduction of 4-NA and 1B-4-NB was completed in 30 s and 60 s respectively (**Fig. 7b, 7c**)

The catalytic efficiency can be defined in terms of the catalytic activity factor (k_a) as shown in **Table 2**. Catalytic activity factor is defined as the ratio of rate constant (k) in s⁻¹ to the amount of catalyst used in mg (Aditya et al. 2017). The catalytic activity factor (k_a) for reduction of 4-NP using Fe₃O₄@trp@Ir nanocatalyst was found to be 1.040 s⁻¹mg⁻¹. The observed catalytic activity factor was higher as compared to the other nanocatalysts in the literature (**Table 2**) suggesting the higher catalytic efficiency of synthesized Fe₃O₄@trp@Ir nanocatalyst. The efficiency of the synthesized nanocatalyst was also determined by calculating the turn over frequency (TOF). The TOF was calculated by dividing the no. of moles of 4-NP consumed by the no. of moles of catalyst used in the reaction per unit time (Nariya et al. 2020). The high TOF obtained for reduction of 4-NP by Fe₃O₄@trp@Ir nanocatalyst (9 min⁻¹) indicates that the catalyst's surface has large no. of active sites which provides effective contact with 4-NP and efficient transfer of electrons from the catalyst surface to 4-NP.

The superior TOF and activity factor for the as-prepared Fe₃O₄@trp@Ir NPs is also attributed to the co-operative effect of two metals (Fe, Ir). The Fe metal in the Fe₃O₄ magnetic particles plays a major role in the enhanced thermal and photostability of Fe₃O₄@trp@Ir NPs, whereas the noble metal Ir effectively participates in the reduction of nitroaromatics. As evidenced by positive Zeta potential values for Fe₃O₄@trp@Ir NPs, the immobilized Ir metal transfers electrons to Fe₃O₄ support to create positively charged surface. The reduction of nitrophenol is a surface phenomenon, therefore accumulation of positive charges on the surface provide suitable environment for the facile reduction of nitrophenol. At present, we do not have solid evidence for the synergistic effect of two metals, but further investigations on understanding the contribution of each metal in enhancing the catalytic activity of the Fe₃O₄@trp@Ir NPs are currently in progress. The proposed mechanism for the 4-NP reduction using Fe₃O₄@trp@Ir nanocatalyst is illustrated in **Scheme 2**. In the first step, BH₄⁻ ions are adsorbed on the nanocatalyst's surface followed by transfer of hydrogen species on the surface of Iridium (Thekkathu et al. 2020). In the second step, the adsorption of 4-nitrophenolate ions took place on the surface of the catalyst. The adsorbed hydrogen species reacts with the adsorbed 4-nitrophenolate ions to form desired 4-AP.

Table 2

Comparison of catalytic activity of Fe₃O₄@trp@Ir nanocatalyst with other reported catalysts for the reduction of nitroaromatics

Entry	Pollutant	Catalyst	C _{cat} (mg/mL)	Time (s)	K _{app} (s ⁻¹)	Activity factor (s ⁻¹ mg ⁻¹)	TOF (min ⁻¹)	Reference
1.	4-NP	Fe ₃ O ₄ @trp@Ir	0.05	20	0.0520	1.040	9	This work
2.	4-NA	Fe ₃ O ₄ @trp@Ir	0.05	30	0.0398	0.796	5.04	This work
3.	1-B-4-NB	Fe ₃ O ₄ @trp@Ir	0.05	60	0.0124	0.246	2.2	This work
4.	4-NP	Fe ₃ O ₄ @trp@Ir	0.025	360	0.0068	0.272	1.12	This work
5.	4-NA	Fe ₃ O ₄ @trp@Ir	0.025	240	0.0059	0.236	1.40	This work
6.	1-B-4-NB	Fe ₃ O ₄ @trp@Ir	0.025	240	0.0039	0.156	1.17	This work
7.	4-NP	AgNPs/SiNSs	0.2	40	0.0801	0.4005	3.52	(Yan et al. 2017)
8.	4-NP	Ag/TP	2.85	540	0.0052	0.0064	3.84	(Ismail et al. 2018)
9.	4-NP	Ag@TPHH-COF	0.02	150	0.022	1.1	4.15	(Wang et al. 2019)
10.	4-NA	Ag@TPHH-COF	0.02	150	0.017	0.85	3.46	(Wang et al. 2019)
11.	4-NP	Fe ₃ O ₄ /Ag@NFC	1	960	0.033	0.033	2.61	(Xiong et al. 2013)
12.	4-NP	Cu/Fe ₃ O ₄ /eggshell	0.14	100	0.0120	0.086	-	(Nasrollahzadeh et al. 2016)
13.	4-NP	micronSiO ₂ @nanoAg	0.25	600	0.0035	0.014	-	(Wang et al. 2013)
14.	4-NP	Fe ₃ O ₄ @TA/Ag	1	60	0.0436	0.044	-	(Veisi et al. 2019)
15.	4-NP	Ir/IrO ₂ @Fe ₃ O ₄	0.25	180	0.0221	0.088	-	(Thekkatu et al. 2020)
16.	4-NA	Ir/IrO ₂ @Fe ₃ O ₄	0.25	180	0.0223	0.089	-	(Thekkatu et al. 2020)

Photocatalytic study

The effect of visible light on the catalytic reduction of 4-NP was also investigated. In the presence of light, photocatalysis and noble metal catalysis plays an important role. However, in dark, the effect of photocatalysis is suppressed (Paquin et al. 2015). The catalytic reduction of 4-NP under the visible light illumination takes only 20 min with conversion efficiency of 95.15% (**Fig. 8b**). The conversion of 4-NP to 4-AP took 40 minutes in the absence of visible light (**Fig. 8a**). The value of the rate constant under visible light illumination is 0.1507 min^{-1} which is about twice the value of the rate constant obtained in dark (0.0755 min^{-1}) (**Fig. 8c**). **Fig. 8d** shows the decrease in absorbance of 4-NP with time under visible light illumination and dark.

The localized surface Plasmon resonance (LSPR) effect of Iridium, enhancement of visible light absorption by Fe_3O_4 nanoparticles, and visible light responsive behavior of the $\text{Fe}_3\text{O}_4@\text{trp}@Ir$ nanocatalyst promote the catalytic process.

The applicability of $\text{Fe}_3\text{O}_4@\text{trp}@Ir$ nanocatalyst was explored in practical applications by testing the reuse ability of the synthesized nanocatalyst. The potential recyclability and the ability to separate the catalyst magnetically are the two main advantages of the synthesized $\text{Fe}_3\text{O}_4@\text{trp}@Ir$ nanocatalyst. The catalyst was magnetically retrieved, washed with DI water, and ethanol, and dried in an oven before using it for the next catalytic cycle. $\text{Fe}_3\text{O}_4@\text{trp}@Ir$ nanocatalyst possesses remarkable stability with the conversion efficiency of 4-NP as high as 89% even after the fifth catalytic cycle as shown in **Fig. 9**.

Conclusion

A simple but effective approach for the preparation of robust and environmentally benign $\text{Fe}_3\text{O}_4@\text{trp}@Ir$ nanocatalyst by co-precipitation method was investigated which could not only catalytically reduce 4-NP but also cause its photocatalytic degradation. The catalyst exhibits remarkable performance in the 4-nitrophenol degradation under visible light illumination. The prepared nanocatalyst possesses important features such as efficient magnetic separation, high stability, and recyclability. The TOF and catalytic activity factor of the $\text{Fe}_3\text{O}_4@\text{trp}@Ir$ nanocatalyst in the reduction of 4-NP is superior to some of the known bimetallic catalysts supported on the Fe_3O_4 . The prepared nanocatalyst's remarkable catalytic activity in the degradation of 4-NP, 4-NA, and 1-B-4-NB is due to the existence of Ir/IrO_2 interfaces. The excellent photocatalytic performance of the novel catalyst makes it a suitable candidate for the environmental remediation process based on photo technology.

Declarations

Funding

The authors declare that no funds, grants were received during the preparation of this manuscript.

Declaration of Competing Interest

The authors declare that they have no known competing financial interests or personal relationships that could have appeared to influence the work reported in this paper. The authors also certify that they have no affiliations with or involvement in any organization.

Author contributions

Diksha: Investigation, Data Curation, Writing- original draft. **Manpreet Kaur:** Conceptualization, Methodology, Writing-original draft. **Veeranna Yempally:** Validation, Supervision, Writing-review, and editing. **Harminder Kaur:** Resources, Supervision, Writing- review, and editing.

Ethics Approval

Not Applicable.

Consent to participate

Informed consent was obtained from all the authors involved.

Consent to publish

The authors have consented for the submission of research work to the Environment Science and Pollution Research Journal.

Data Availability Statements

The authors declare that all relevant data are included in the manuscript.

Acknowledgements:

Diksha would like to acknowledge PEC and MHRD for providing GATE fellowship.

References

- Aditya T, Jana J, Singh NK, et al (2017) Remarkable Facet Selective Reduction of 4-Nitrophenol by Morphologically Tailored (111) Faceted Cu₂O Nanocatalyst. ACS Omega 2:1968–1984. <https://doi.org/10.1021/acsomega.6b00447>
- Alaghmandfard A, Madaah Hosseini HR (2021) A facile, two-step synthesis and characterization of Fe₃O₄-L-Cysteine-graphene quantum dots as a multifunctional nanocomposite. Appl Nanosci 11:849–860. <https://doi.org/10.1007/s13204-020-01642-1>
- Babajani N, Jamshidi S (2019) Investigation of photocatalytic malachite green degradation by iridium doped zinc oxide nanoparticles: Application of response surface methodology. J Alloys Compd 782:533–544. <https://doi.org/10.1016/j.jallcom.2018.12.164>
- Bagbi Y, Sarswat A, Mohan D, et al (2017) Lead and Chromium Adsorption from Water using L-Cysteine Functionalized Magnetite (Fe₃O₄) Nanoparticles. Sci Rep 7:1–15. <https://doi.org/10.1038/s41598-017-03380-x>
- Banerjee S, Benjwal P, Singh M, Kar KK (2018) Graphene oxide (rGO)-metal oxide (TiO₂/Fe₃O₄) based nanocomposites for the removal of methylene blue. Appl Surf Sci 439:560–568. <https://doi.org/10.1016/j.apsusc.2018.01.085>
- Basavegowda N, Mishra K, Lee YR (2017) Trimetallic FeAgPt alloy as a nanocatalyst for the reduction of 4-nitroaniline and decolorization of rhodamine B: A comparative study. J Alloys Compd 701:456–464. <https://doi.org/10.1016/j.jallcom.2017.01.122>
- Belachew N, Tadesse A, Kahsay MH, et al (2021) Synthesis of amino acid functionalized Fe₃O₄ nanoparticles for adsorptive removal of Rhodamine B. Appl Water Sci 11:1–9. <https://doi.org/10.1007/s13201-021-01371-y>
- Boruah PK, Borah DJ, Handique J, et al (2015) Facile synthesis and characterization of Fe₃O₄ nanopowder and Fe₃O₄/reduced graphene oxide nanocomposite for methyl blue adsorption: A comparative study. J Environ Chem Eng 3:1974–1985. <https://doi.org/10.1016/j.jece.2015.06.030>

- Chi Y, Yuan Q, Li Y, et al (2012) Synthesis of Fe₃O₄@SiO₂-Ag magnetic nanocomposite based on small-sized and highly dispersed silver nanoparticles for catalytic reduction of 4-nitrophenol. *J Colloid Interface Sci* 383:96–102. <https://doi.org/10.1016/j.jcis.2012.06.027>
- Chishti AN, Guo F, Aftab A, et al (2021) Synthesis of silver doped Fe₃O₄/C nanoparticles and its catalytic activities for the degradation and reduction of methylene blue and 4-nitrophenol. *Appl Surf Sci* 546:149070. <https://doi.org/10.1016/j.apsusc.2021.149070>
- Cui M, Huang X, Zhang X, et al (2020) Ultra-small iridium nanoparticles as active catalysts for the selective and efficient reduction of nitroarenes. *New J Chem* 44:18274–18280. <https://doi.org/10.1039/d0nj03621h>
- Dhanalakshmi M, Lakshmi Prabavathi S, Saravanakumar K, et al (2020) Iridium nanoparticles anchored WO₃ nanocubes as an efficient photocatalyst for removal of refractory contaminants (crystal violet and methylene blue). *Chem Phys Lett* 745:137285. <https://doi.org/10.1016/j.cplett.2020.137285>
- Dinari M, Dadkhah F (2021) Visible light photodegradation of 4-nitrophenol by new high-performance and easy recoverable Fe₃O₄/Ag₂O-LDH hybrid photocatalysts. *Appl Organomet Chem* 35:1–13. <https://doi.org/10.1002/aoc.6355>
- Dutta S, Sarkar S, Ray C, et al (2014) Mesoporous gold and palladium nanoleaves from liquid-liquid interface: Enhanced catalytic activity of the palladium analogue toward hydrazine-assisted room-temperature 4-nitrophenol reduction. *ACS Appl Mater Interfaces* 6:9134–9143. <https://doi.org/10.1021/am503251r>
- Fagiolari L, Bini M, Costantino F, et al (2020) Iridium-Doped Nanosized Zn-Al Layered Double Hydroxides as Efficient Water Oxidation Catalysts. *ACS Appl Mater Interfaces* 12:32736–32745. <https://doi.org/10.1021/acsami.0c07925>
- Feng J, Lv F, Zhang W, et al (2017) Iridium-Based Multimetallic Porous Hollow Nanocrystals for Efficient Overall-Water-Splitting Catalysis. *Adv Mater* 29:1–8. <https://doi.org/10.1002/adma.201703798>
- Goel A, Lasyal R (2016) Iridium nanoparticles with high catalytic activity in degradation of acid red-26: An oxidative approach. *Water Sci Technol* 74:2551–2559. <https://doi.org/10.2166/wst.2016.330>
- Hung CM, Chen CW, Jhuang YZ, Dong C Di (2016) Fe₃O₄ magnetic nanoparticles: Characterization and performance exemplified by the degradation of methylene blue in the presence of persulfate. *J Adv Oxid Technol* 19:43–51. <https://doi.org/10.1515/jaots-2016-0105>
- Ismail M, Khan MI, Khan SB, et al (2018) Catalytic reduction of picric acid, nitrophenols and organic azo dyes via green synthesized plant supported Ag nanoparticles. *J Mol Liq* 268:87–101. <https://doi.org/10.1016/j.molliq.2018.07.030>
- Kapkowski M, Ambrożkiewicz W, Siudyga T, et al (2017) Nano silica and molybdenum supported Re, Rh, Ru or Ir nanoparticles for selective solvent-free glycerol conversion to cyclic acetals with propanone and butanone under mild conditions. *Appl Catal B Environ* 202:335–345. <https://doi.org/10.1016/j.apcatb.2016.09.032>
- Kianfar AH, Arayesh MA (2020) Synthesis, characterization and investigation of photocatalytic and catalytic applications of Fe₃O₄/TiO₂/CuO nanoparticles for degradation of MB and reduction of nitrophenols. *J Environ Chem Eng* 8:103640. <https://doi.org/10.1016/j.jece.2019.103640>
- Kumari M, Gupta R, Jain Y (2019) Fe₃O₄ – Glutathione stabilized Ag nanoparticles: A new magnetically separable robust and facile catalyst for aqueous phase reduction of nitroarenes. *Appl Organomet Chem* 33:1–11. <https://doi.org/10.1002/aoc.5223>

- Kundu S, Liang H (2011) Shape-selective formation and characterization of catalytically active iridium nanoparticles. *J Colloid Interface Sci* 354:597–606. <https://doi.org/10.1016/j.jcis.2010.11.032>
- Mancuso A, Navarra W, Sacco O, et al (2021) Photocatalytic degradation of thiacloprid using tri-doped TiO_2 photocatalysts: A preliminary comparative study. *Catalysts* 11:. <https://doi.org/10.3390/catal11080927>
- Mihaela R, Barbu-tudoran L, Oancea S, et al (2022) Aspartic Acid Stabilized Iron Oxide Nanoparticles for Biomedical Applications
- Moeini N, Tamoradi T, Ghadermazi M, Ghorbani-Choghamarani A (2018) Anchoring Ni (II) on Fe_3O_4 @tryptophan: A recyclable, green and extremely efficient magnetic nanocatalyst for one-pot synthesis of 5-substituted 1H-tetrazoles and chemoselective oxidation of sulfides and thiols. *Appl Organomet Chem* 32:1–12. <https://doi.org/10.1002/aoc.4445>
- Mohamed MM, Al-Sharif MS (2013) Visible light assisted reduction of 4-nitrophenol to 4-aminophenol on Ag/TiO_2 photocatalysts synthesized by hybrid templates. *Appl Catal B Environ* 142–143:432–441. <https://doi.org/10.1016/j.apcatb.2013.05.058>
- Mondal A, Mondal A, Adhikary B, Mukherjee DK (2017) Cobalt nanoparticles as reusable catalysts for reduction of 4-nitrophenol under mild conditions. *Bull Mater Sci* 40:321–328. <https://doi.org/10.1007/s12034-017-1367-3>
- Muntean R, Pascal DT, Rost U, et al (2019) Investigation of Iridium Nanoparticles Supported on Sub-stoichiometric Titanium Oxides as Anodic Electrocatalysts in PEM Electrolysis. Part I.: Synthesis and Characterization. *Top Catal* 62:429–438. <https://doi.org/10.1007/s11244-019-01164-3>
- Nariya P, Das M, Shukla F, Thakore S (2020) Synthesis of magnetic silver cyclodextrin nanocomposite as catalyst for reduction of nitro aromatics and organic dyes. *J Mol Liq* 300:112279. <https://doi.org/10.1016/j.molliq.2019.112279>
- Nasir Baig RB, Varma RS (2013) Magnetic silica-supported ruthenium nanoparticles: An efficient catalyst for transfer hydrogenation of carbonyl compounds. *ACS Sustain Chem Eng* 1:805–809. <https://doi.org/10.1021/sc400032k>
- Nasrollahzadeh M, Sajadi SM, Hatamifard A (2016) Waste chicken eggshell as a natural valuable resource and environmentally benign support for biosynthesis of catalytically active $\text{Cu}/\text{eggshell}$, $\text{Fe}_3\text{O}_4/\text{eggshell}$ and $\text{Cu}/\text{Fe}_3\text{O}_4/\text{eggshell}$ nanocomposites. *Appl Catal B Environ* 191:209–227. <https://doi.org/10.1016/j.apcatb.2016.02.042>
- Ohno H, Nohara S, Kakinuma K, et al (2017) Remarkable Mass Activities for the Oxygen Evolution Reaction at Iridium Oxide Nanocatalysts Dispersed on Tin Oxides for Polymer Electrolyte Membrane Water Electrolysis. *J Electrochem Soc* 164:F944–F947. <https://doi.org/10.1149/2.1101709jes>
- Paquin F, Rivnay J, Salleo A, et al (2015) Multi-phase semicrystalline microstructures drive exciton dissociation in neat plastic semiconductors. *J Mater Chem C* 3:10715–10722. <https://doi.org/10.1039/b000000x>
- Paul A, Dhar SS (2020) Designing $\text{Cu}_2\text{V}_2\text{O}_7/\text{CoFe}_2\text{O}_4/\text{g-C}_3\text{N}_4$ ternary nanocomposite: A high performance magnetically recyclable photocatalyst in the reduction of 4-nitrophenol to 4-aminophenol. *J Solid State Chem* 290:121563. <https://doi.org/10.1016/j.jssc.2020.121563>
- Pav AI, Galindo E, Paraguay-delgado F, et al (2020) Magnetic nanocomposite with fluorescence enhancement effect based on amino acid coated- Fe_3O_4 functionalized with quantum dots. 251:. <https://doi.org/10.1016/j.matchemphys.2020.123082>

Pham MT, Hussain A, Bui DP, et al (2021) Surface plasmon resonance enhanced photocatalysis of Ag nanoparticles-decorated Bi₂S₃ nanorods for NO degradation. *Environ Technol Innov* 23:101755.

<https://doi.org/10.1016/j.eti.2021.101755>

Priya DB, Asharani IV (2018) Catalytic reduction in 4-nitrophenol using Actinodaphne madraspatana Bedd leaves-mediated palladium nanoparticles. *IET Nanobiotechnology* 12:116–126. <https://doi.org/10.1049/iet-nbt.2017.0027>

Rawat J, Bijalwan K, Negi C, et al (2021) Magnetically recoverable Au doped iron oxide nanoparticles coated with graphene oxide for catalytic reduction of 4-nitrophenol. *Mater Today Proc* 45:4869–4873.

<https://doi.org/10.1016/j.matpr.2021.01.349>

Samuel MS, Jose S, Selvarajan E, et al (2020) Biosynthesized silver nanoparticles using *Bacillus amyloliquefaciens*; Application for cytotoxicity effect on A549 cell line and photocatalytic degradation of p-nitrophenol. *J Photochem Photobiol B Biol* 202:111642. <https://doi.org/10.1016/j.jphotobiol.2019.111642>

<https://doi.org/10.1016/j.jphotobiol.2019.111642>

Seoudi R, Al-Marhaby FA (2016) Synthesis, Characterization and Photocatalytic Application of Different Sizes of Gold Nanoparticles on 4-Nitrophenol. *World J Nano Sci Eng* 06:120–128. <https://doi.org/10.4236/wjnse.2016.63012>

Shabib F, Fazaeli R, Aliyan H, Richeson D (2022) Hierarchical mesoporous plasmonic Pd-Fe₃O₄/NiFe-LDH composites: Characterization, and kinetic study of a photodegradation catalyst for aqueous metoclopramide. *Environ Technol Innov* 27:102515. <https://doi.org/10.1016/j.eti.2022.102515>

<https://doi.org/10.1016/j.eti.2022.102515>

Sharif HMA, Mahmood A, Cheng HY, et al (2019) Fe₃O₄ Nanoparticles Coated with EDTA and Ag Nanoparticles for the Catalytic Reduction of Organic Dyes from Wastewater. *ACS Appl Nano Mater* 2:5310–5319.

<https://doi.org/10.1021/acsanm.9b01250>

Theerdhala S, Bahadur D, Vitta S, et al (2010) Sonochemical stabilization of ultrafine colloidal biocompatible magnetite nanoparticles using amino acid, l-arginine, for possible bio applications. *Ultrason Sonochem* 17:730–737.

<https://doi.org/10.1016/j.ultsonch.2009.12.007>

Thekkathu R, Ashok D, K Ramkollath P, et al (2020) Magnetically recoverable Ir/IrO₂@Fe₃O₄ core/ SiO₂ shell catalyst for the reduction of organic pollutants in water. *Chem Phys Lett* 742:137147. <https://doi.org/10.1016/j.cplett.2020.137147>

<https://doi.org/10.1016/j.cplett.2020.137147>

Tie SL, Lin YQ, Lee HC, et al (2006) Amino acid-coated nano-sized magnetite particles prepared by two-step transformation. *Colloids Surfaces A Physicochem Eng Asp* 273:75–83. <https://doi.org/10.1016/j.colsurfa.2005.08.027>

Tipsawat P, Wongpratut U, Phumying S, et al (2018) Magnetite (Fe₃O₄) nanoparticles: Synthesis, characterization and electrochemical properties. *Appl Surf Sci* 446:287–292. <https://doi.org/10.1016/j.apsusc.2017.11.053>

<https://doi.org/10.1016/j.apsusc.2017.11.053>

Veisi H, Moradi SB, Saljooqi A, Safarimehr P (2019) Silver nanoparticle-decorated on tannic acid-modified magnetite nanoparticles (Fe₃O₄@TA/Ag) for highly active catalytic reduction of 4-nitrophenol, Rhodamine B and Methylene blue. *Mater Sci Eng C* 100:445–452. <https://doi.org/10.1016/j.msec.2019.03.036>

<https://doi.org/10.1016/j.msec.2019.03.036>

Wang M, Tian D, Tian P, Yuan L (2013) Synthesis of micron-SiO₂@nano-Ag particles and their catalytic performance in 4-nitrophenol reduction. *Appl Surf Sci* 283:389–395. <https://doi.org/10.1016/j.apsusc.2013.06.120>

<https://doi.org/10.1016/j.apsusc.2013.06.120>

Wang RL, Li DP, Wang LJ, et al (2019) The preparation of new covalent organic framework embedded with silver nanoparticles and its applications in degradation of organic pollutants from waste water. *Dalt Trans* 48:1051–1059.

<https://doi.org/10.1039/C8DT04458A>

Xiong R, Lu C, Wang Y, et al (2013) Nanofibrillated cellulose as the support and reductant for the facile synthesis of Fe₃O₄/Ag nanocomposites with catalytic and antibacterial activity. *J Mater Chem A* 1:14910–14918.
<https://doi.org/10.1039/c3ta13314a>

Xu D, Diao P, Jin T, et al (2015) Iridium Oxide Nanoparticles and Iridium/Iridium Oxide Nanocomposites: Photochemical Fabrication and Application in Catalytic Reduction of 4-Nitrophenol. *ACS Appl Mater Interfaces* 7:16738–16749.
<https://doi.org/10.1021/acsami.5b04504>

Yan Z, Fu L, Zuo X, Yang H (2017) PT Graphical Abstract SC. "Applied Catal B, Environ."
<https://doi.org/10.1016/j.apcatb.2017.12.040>

Zhang RL, Duan JJ, Mei LP, et al (2020) Facile synthesis of porous iridium-palladium-plumbum wire-like nanonetworks with boosted catalytic performance for hydrogen evolution reaction. *J Colloid Interface Sci* 580:99–107.
<https://doi.org/10.1016/j.jcis.2020.06.124>

Zhao F, Khaing KK, Yin D, et al (2018) Large enhanced photocatalytic activity of g-C₃N₄ by fabrication of a nanocomposite with introducing upconversion nanocrystal and Ag nanoparticles. *RSC Adv* 8:42308–42321.
<https://doi.org/10.1039/c8ra07901c>

Schemes

Schemes 1-2 are in the supplementary files section.

Figures

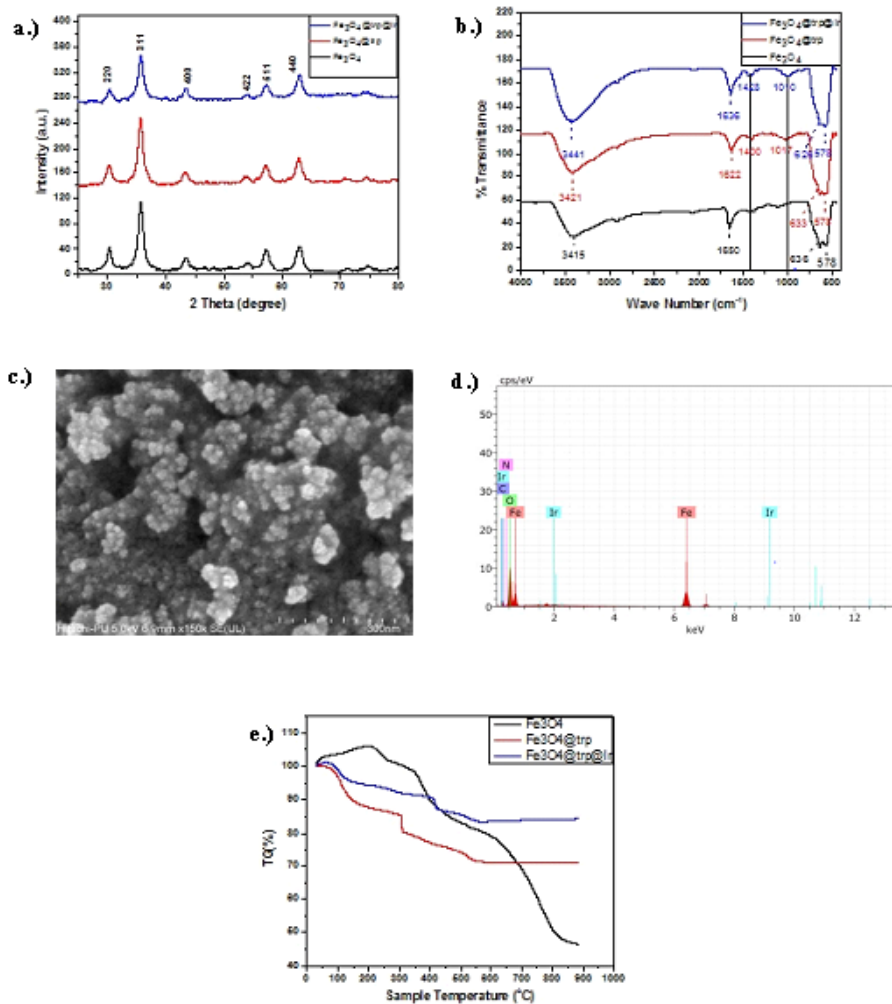


Figure 1

a) XRD pattern of as-prepared nanocatalyst, b) FTIR spectra, c) FE-SEM image of Fe₃O₄@trp@Ir, d) EDX of Fe₃O₄@trp@Ir, e) TGA analysis

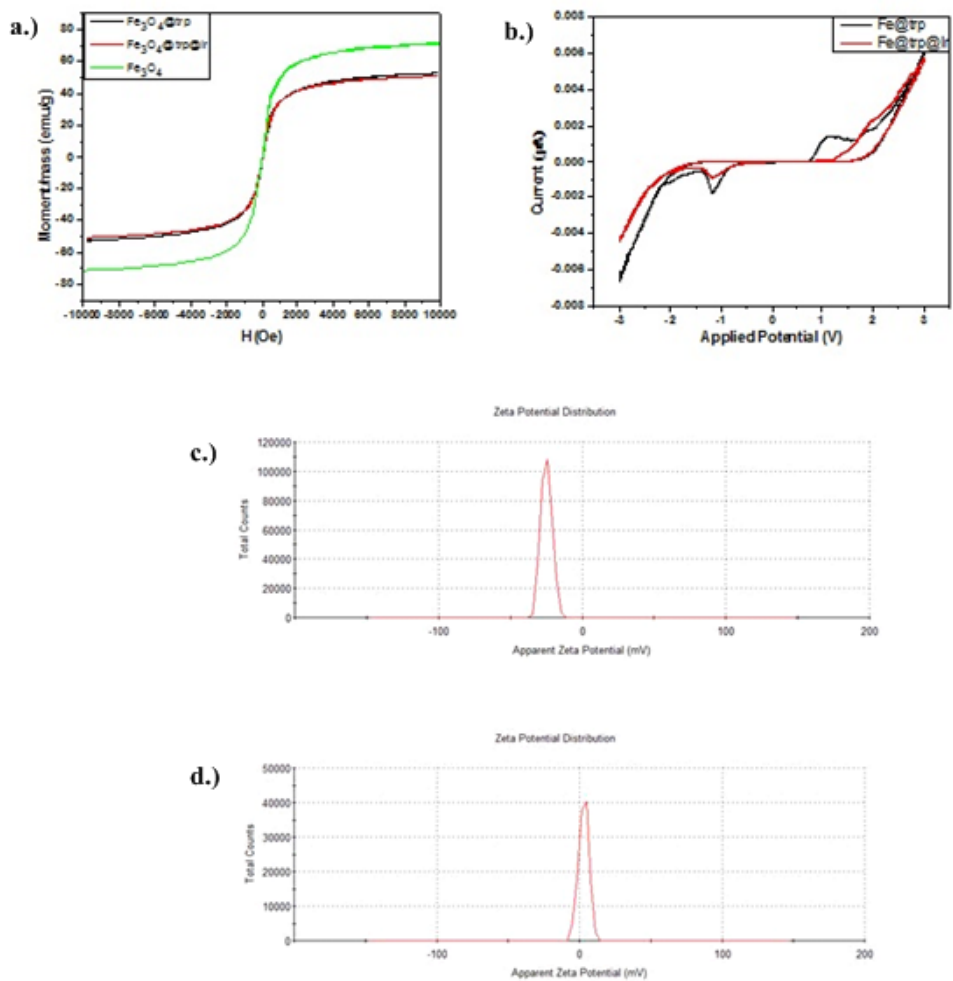


Figure 2

a) VSM of Fe_3O_4 , $\text{Fe}_3\text{O}_4@trp$, and $\text{Fe}_3\text{O}_4@trp@Ir$, b) CV graph of $\text{Fe}_3\text{O}_4@trp$ and $\text{Fe}_3\text{O}_4@trp@Ir$, c.) Zeta potential of $\text{Fe}_3\text{O}_4@trp$, d.) Zeta potential of $\text{Fe}_3\text{O}_4@trp@Ir$

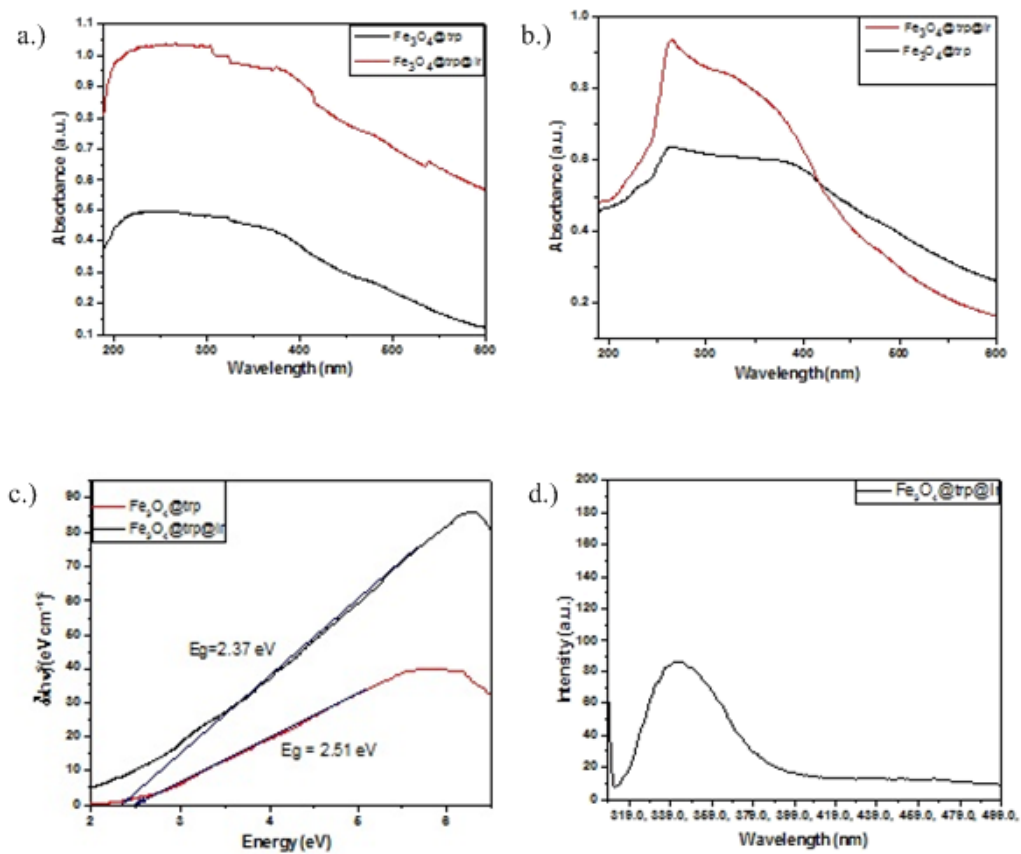


Figure 3

a.) Absorbance of nanoparticles from UV-Vis DRS measurements, b.) UV-Vis absorption spectra of $\text{Fe}_3\text{O}_4@\text{trp}$ and $\text{Fe}_3\text{O}_4@\text{trp}@Ir$ in DMSO, c.) Tauc plot of synthesized nanoparticles, d.) PL emission spectra of $\text{Fe}_3\text{O}_4@\text{trp}@Ir$.

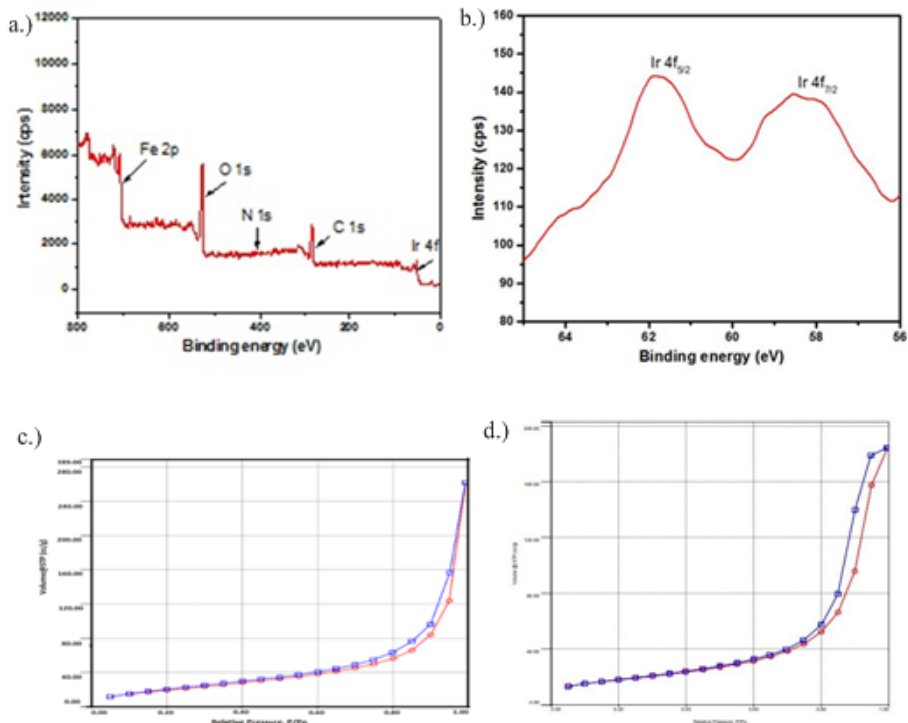


Figure 4

a.) XPS survey scan of Fe₃O₄@trp@Ir nanocatalyst, b.) High-resolution XPS spectra of Ir4f, c.) N₂ adsorption-desorption isotherms of Fe₃O₄@trp@Ir nanocatalyst, d.) Adsorption-desorption isotherms of Fe₃O₄ nanoparticles

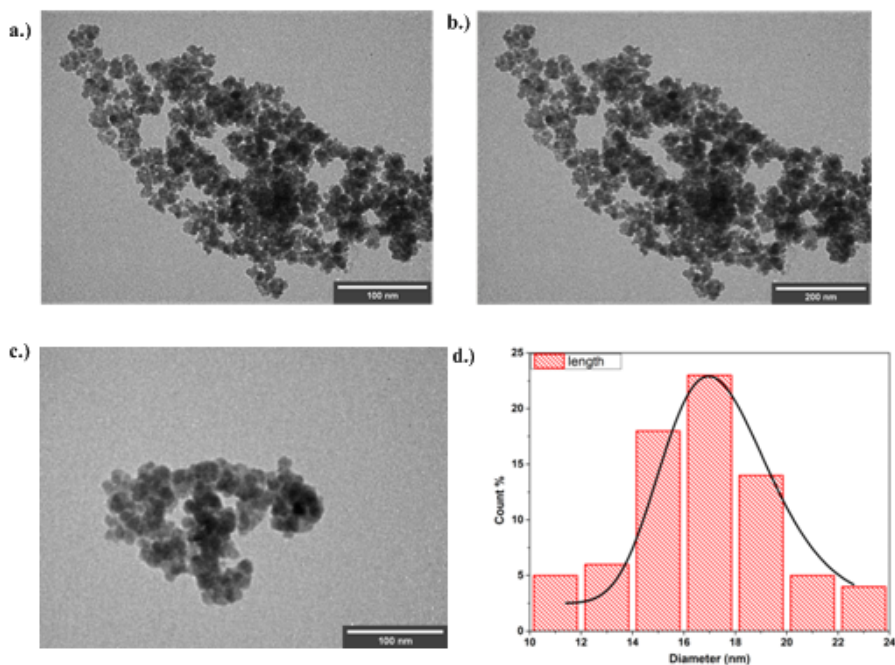


Figure 5

TEM images of Fe₃O₄@trp@Ir nanocatalyst (a,b,c) and particle size distribution (d).

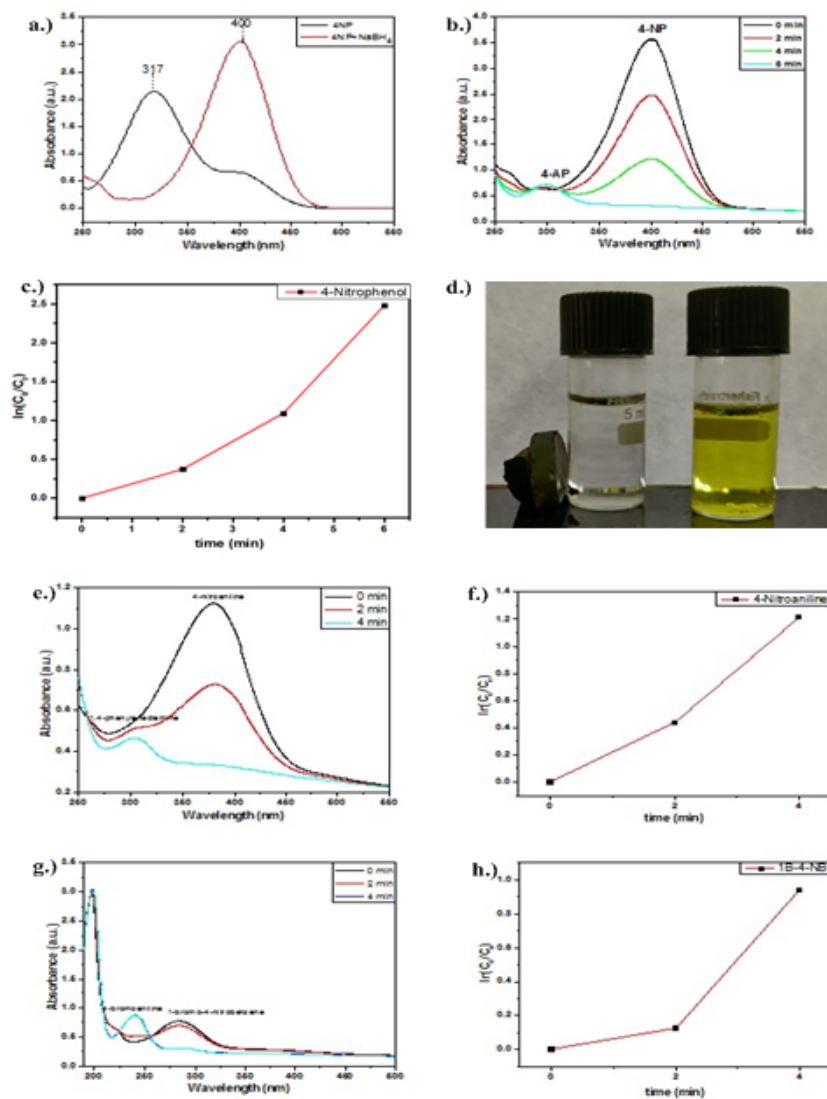


Figure 6

a) UV-vis spectra of 4-NP and 4-NP+NaBH₄ b) reduction of 4-NP using 0.025mg/mL of Fe₃O₄@trp@Ir catalyst c) Pseudo-first order kinetics of 4-NP d) Magnetic separation of catalyst and formation of 4-AP e) Reduction of 4-NA using 0.025 mg/mL nanocatalyst f) Pseudo-first order kinetics of 4-NA g.) Reduction of 1-B-4-NB and h.) Pseudo-first order kinetics

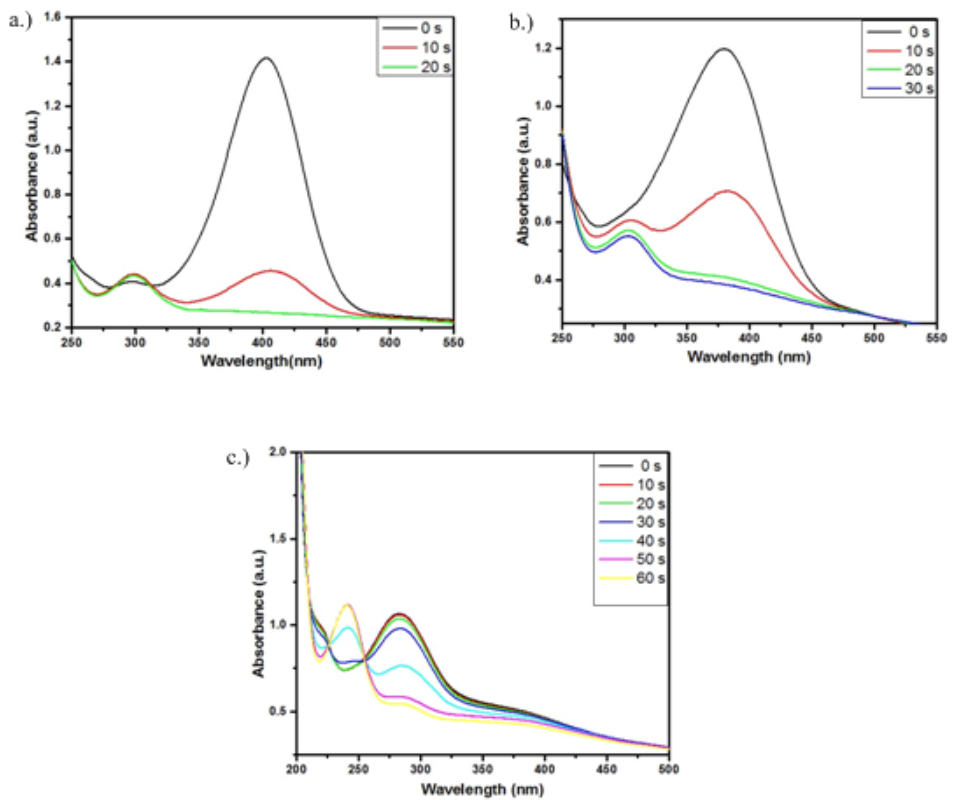


Figure 7

a.) Reduction of 4-NP using 0.05 mg/mL $\text{Fe}_3\text{O}_4@\text{trp}@\text{Ir}$ catalyst, b.) Reduction of 4-NA using 0.05 mg/mL nanocatalyst
 c.) Reduction of 1B-4-NB using 0.05 mg/mL nanocatalyst

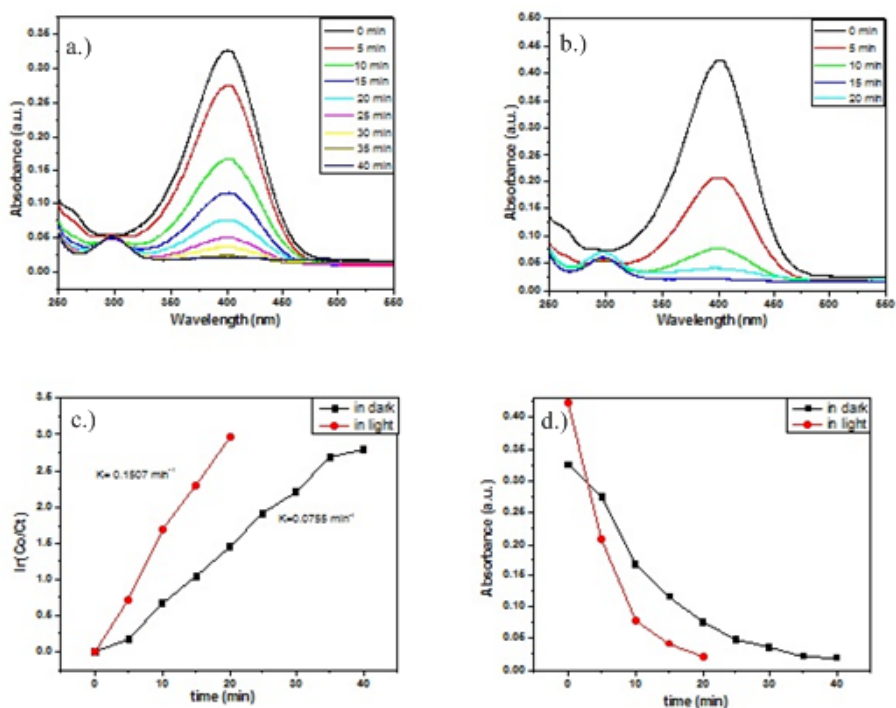


Figure 8

a-d Experimental details for the visible light-assisted photodegradation of 4-NP by $\text{Fe}_3\text{O}_4@\text{trp}@\text{Ir}$ nanocatalyst a.) Time-dependent UV-vis spectra of 4-NP recorded in dark and b.) in light, c.) Plot showing $\ln(\text{Co}/\text{Ct})$ vs time d.) The plot of absorbance vs time. Reaction Conditions: $[\text{4-NP}] = 50 \text{ ml of } 0.1 \text{ mmol L}^{-1}$, $[\text{NaBH}_4] = 5 \text{ ml of } 0.05 \text{ M}$, amount of catalyst used = 0.005 g.

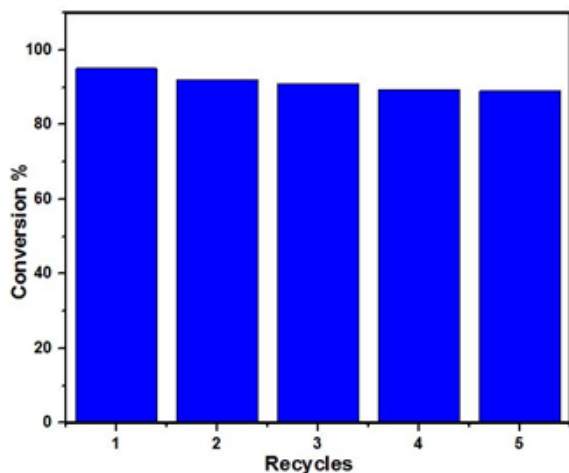


Figure 9

Illustration of conversion% of 4-NP upto 5 repeated cycles using $\text{Fe}_3\text{O}_4@\text{trp}@\text{Ir}$ nanocatalyst. Reaction Conditions: $[\text{4-NP}] = 50 \text{ ml of } 0.1 \text{ mmol L}^{-1}$, $[\text{NaBH}_4] = 5 \text{ ml of } 0.05 \text{ M}$, amount of catalyst used = 0.005 g.

Supplementary Files

This is a list of supplementary files associated with this preprint. Click to download.

- [scheme1.jpg](#)
- [scheme2.jpg](#)